Original Article

Determination of dosimetric leaf gap using amorphous silicon electronic portal imaging device and its influence on intensity modulated radiotherapy dose delivery

S. Timothy Peace Balasingh, I. Rabi Raja Singh, K. Mohamathu Rafic, S. Ebenezer Suman Babu, B. Paul Ravindran

Department of Radiotherapy, Christian Medical College, Vellore, Tamil Nadu, India

Received on: 27-12-2014 Review completed on: 06-04-2015 Accepted on: 13-04-2015

ABSTRACT

As complex treatment techniques such as intensity modulated radiotherapy (IMRT) entail the modeling of rounded leaf-end transmission in the treatment planning system, it is important to accurately determine the dosimetric leaf gap (DLG) value for a precise calculation of dose. The advancements in the application of the electronic portal imaging device (EPID) in quality assurance (QA) and dosimetry have facilitated the determination of DLG in this study. The DLG measurements were performed using both the ionization chamber (DLG_{ion}) and EPID (DLG_{EPID}) for sweeping gap fields of different widths. The DLG_{ion} values were found to be 1.133 mm and 1.120 mm for perpendicular and parallel orientations of the 0.125 cm^3 ionization chamber, while the corresponding DLG_{EPID} values were 0.843 mm and 0.819 mm, respectively. It was found that the DLG was independent of volume and orientation of the ionization chamber, depth, source to surface distance (SSD), and the rate of dose delivery. Since the patient-specific QA tests showed comparable results between the IMRT plans based on the DLG_{EPID} and DLG_{ion}, it is concluded that the EPID can be a suitable alternative in the determination of DLG.

Key words: Dosimetric leaf gap, electronic portal imaging device, intensity modulated radiotherapy, MLC transmission, rounded leaf-end transmission, sweeping gap

Introduction

The introduction of multileaf collimators (MLC), reported since the late eighties,[1-3] has revolutionized radiation therapy, ushering in the concept of conformal therapy while paving the way for rapid development of newer treatment techniques that have improved the efficacy of delivery and the resultant outcomes.

Address for correspondence:
Mr. S. Timothy Peace Balasingh,
Department of Radiotherapy, Christian Medical College,
Vellore - 632 004, Tamil Nadu, India.
E-mail: tim_peace@yahoo.co.in

Access this article online	
Quick Response Code:	Website: www.jmp.org.in
	DOI: 10.4103/0971-6203.165072

The MLC systems that are commercially available primarily differ from one another in the tongue and groove and leaf-end designs. The single-focused leaves are rounded at the tip vertically so as to attain better off-axis dosimetric characteristics such as constant penumbra at the plane of the isocenter across the field.[4] This results in the rounded leaf-end transmission where radiation passes between the leaves even when they are closed. Though the rounded-end leaves have an advantage over their double-focused counterparts (obeying beam divergence), the ensuing leaf-end transmission brings in a complexity in the beam modeling that can radically affect the dose calculation in model-based treatment planning systems (TPS).

How to cite this article: Balasingh ST, Singh IR, Rafic KM, Babu SE, Ravindran BP. Determination of dosimetric leaf gap using amorphous silicon electronic portal imaging device and its influence on intensity modulated radiotherapy dose delivery. J Med Phys 2015;40:129-35.

The leakage through the rounded leaf-ends, more relevant in dynamic intensity modulated radiotherapy (d-IMRT) delivery as compared to "step and shoot" delivery, has to be accurately accounted for in order to avoid erroneous dose delivery.[5] During the leaf-sequencing process of IMRT planning, the leaf motion calculator (LMC) which converts the optimal fluence into leaf sequences that can be achieved by the MLC,[6] accounts for the transmission of radiation through the two abutting rounded leaves as specified by the dosimetric leaf gap (DLG).

The dose calculation algorithm of the Eclipse™ TPS, which models the leaf-ends as square instead of round, incorporates the DLG parameter that accounts for the leaf transmission by moving the positions of the leaf tips while calculating the actual fluence. Each leaf tip of the MLC leaf pair is moved back by half the DLG value, in such a way that the separation between a completely closed leaf pair is equal to the DLG value.[7] The actual fluence is calculated by the LMC that corrects the optimal fluence generated by the optimization algorithm for the calculated leaf sequence and also accounting for transmission, leakage factors, minimum leaf gap, and leaf speed and span.[8,9] Since the delivery of IMRT depends on the ability of the TPS to model the dynamic MLC (d-MLC) beam both geometrically and dosimetrically in a precise manner,[10] it is important to accurately determine the DLG value.

Clark *et al.*[11] measured the DLG using sweeping gap fields of different widths and plotting the net dose against the gap width as part of the TPS commissioning. The sweeping gap fields enable the dynamic motion of MLC leaves with a constant gap across the reference field set by the jaws to deliver a uniform dose. These were first used by LoSasso *et al.*[5] for verifying leaf gap accuracy.

Zygmanski *et al.*[12] developed a generalized model to simultaneously calculate MLC parameters such as direct MLC transmission, MLC scatter correction, and DLG. The DLG was calculated as the sum of the center mechanical offset and twice the radiation field offset that is the MLC position offset due to the transmission through the rounded leaf-ends. The use of measured DLG to check the dosimetric reproducibility of d-IMRT plans was investigated by Mei *et al.*[13] using the ionization chamber for point dose measurements, amorphous silicon (a-Si) electronic portal imaging device (EPID) for two-dimensional (2D) measurements, and a one-dimensional diode array.

Essers *et al.*[14] performed several tests to check the suitability of d-MLC mode in combination with an inverse planning system and LMC software for clinical use. They varied the MLC transmission and DLG values and determined the optimal values by measuring the absolute dose profiles. The DLG values obtained from five different centers were compared by Van Esch *et al.*[9] by performing measurements using different techniques and detectors such as an ionization chamber, a diamond detector, and film.

The EPID, introduced initially as a reliable replacement for portal films,[15] and more recently in quality assurance (QA)[16-19] and dosimetry,[20-24] has become an active area of research with the introduction of a-Si based flat panel detectors.[25-28] The a-Si detector panel is a matrix of light-sensitive photodiodes for integrating the light and thin-film transistors which act as the switch to the readout electronics.

While most of the published DLG studies have focused primarily on the measurement of DLG as part of the IMRT commissioning process,[9,11,14] few authors have investigated the dosimetric parameters affecting the DLG and its influence on dose calculation and delivery.[12,13] In this study, the use of an a-Si EPID as an alternative to the ionization chamber for the measurement of the DLG has been investigated. The influence of the interleaf and intraleaf leakage patterns observed from the dose maps of the sweeping gap fields acquired using the EPID have been demonstrated. DLG_{EPID} measurements were performed, simulating the ionization chambers of different volumes and orientations. Further, the influence of medium and depth of measurement on the DLG were studied. Finally, the impact of DLG_{ion} and DLG_{EPID} on IMRT dose delivery was also investigated using patient-specific QA tests viz., central axis (CAX) absolute dosimetry and fluence verification using portal dosimetry.

Materials and Methods

The 6 MV photon beam of the Clinac 2100C/D dual-energy linear accelerator equipped with a 120-leaf Millennium multi-leaf collimator system and an aS1000 EPID (Varian Medical Systems, Inc., USA) was used in this study. In order to measure the DLG, sweeping gap fields of varying widths were used. To measure the MLC leakage, two completely blocked MLC fields (one with MLC bank A completely closing the field, as shown in Figure 1, and the other with MLC bank B closed in a similar manner) were employed since a single blocked field with both MLC banks closed at the center would result in over-estimating the MLC leakage due to the abutting leaf-end transmission. A plan was created in Eclipse™ TPS (Varian Medical Systems, Inc., USA) consisting of seven sweeping gap fields of widths 2 mm, 4 mm, 6 mm, 10 mm, 14 mm, 16 mm, and 20 mm, respectively, apart from two closed MLC fields and an open field. A reference field size of 10 cm × 10 cm was set by the X and Y jaws for all the above ten fields, which will hereafter be referred to as DLG fields. Each sweeping gap traveled across this reference field, and had a control point for every centimeter. The leaf sequences for the same were calculated using LMC.

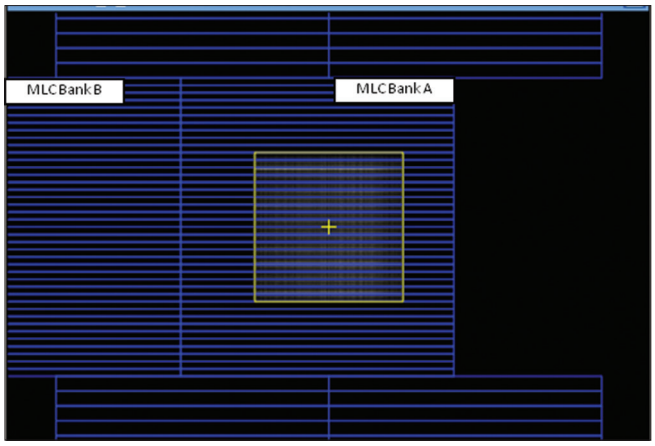

Figure 1: The beam's eye view projection of the completely blocked multileaf collimator (MLC) field with MLC bank A closed

Determination of Dosimetric Leaf Gap

The DLG plan (consisting of the DLG fields) was irradiated on the linear accelerator and the doses for DLG fields were measured using both the ionization chamber and EPID. Each DLG field had a constant monitor unit setting (MU) of 100 MU, which was delivered at a dose rate (pulse rate) of 400 MU/min. The DLG was obtained from the graph in which the output factor ($R_{sg,\ w}$) corrected for MLC leakage is plotted against its sweeping gap width (w).

The output factor, $R_{sg,\ w} = D_{sg,\ w}/D_{open}$

Where, $D_{sg,\ w}$ is the dose measured for sweeping field (w) and D_{open} is the dose measured for open field.

The MLC transmission was calculated as the ratio of the dose measured with the MLC in closed and open positions for the reference field size. The former was obtained by taking the mean of the doses thrice measured with each MLC bank completely closed. However, in order to accurately determine the MLCT for the time for which the MLC leaves block the detector for each sweeping gap field, the corrected MLCT was calculated using the following formula.[13]

Corrected MLCT = MLCT × (1−(w/L))

Where L is the distance (100 mm) traveled by the MLCs for each sweeping gap field.

The corrected output factor ($R_{c,\ sg,\ w}$), obtained by subtracting the corrected MLCT from $R_{sg,\ w}$, was plotted against the sweeping gap width "w", and the DLG was derived as the x-intercept of the linear extrapolation.[5]

DLG_{ion} Study

The DLG_{ion} measurements were recorded three times using the 0.125 cm^3 Semiflex ionization chamber (PTW, Germany) "in water" on the MP3-S radiation field analyzer (RFA, PTW, Germany), except where stated otherwise. The chamber was placed at d_{max} (1.5 cm), with source to surface distance (SSD) of 103.5 cm [Figure 2] to aid comparison with the DLG_{EPID} measurements, which were acquired with the EPID at a source to detector distance (SDD) of 105 cm.

Since the doses measured for the DLG fields include contributions from interleaf and intraleaf leakage, the volume and orientation of the ionization chamber could influence the dose measurement, and hence the DLG_{ion} value. To understand the influence of chamber orientation on DLG determination, the DLG measurements were performed with the 0.125 cm^3 ionization chamber in three orientations viz., perpendicular and parallel to the direction of the sweeping beam and parallel to the CAX. Due to the limitation of the RFA, the chamber could not be physically positioned in the first orientation; instead, the collimator was rotated by 90°.

In order to study the effect of chamber volume, the DLG_{ion} measurements were repeated using the 0.6 cm^3 Farmer-type ionization chamber (PTW, Germany), positioned in the first two orientations, on a 40 cm × 40 cm × 40 cm water phantom. To investigate the influence of the medium of measurement on DLG_{ion}, measurements were carried out using this chamber "in air" with a brass buildup.

To study the influence of depth on DLG_{ion}, measurements were recorded with the ionization chamber positioned at 1.5 cm, 5 cm, and 10 cm, respectively, with SSD of 100 cm. Since the leaf speed increases with an increase in the rate of dose delivery for constant MU settings, it is important to study the effect of dose rate on DLG. The dependence of DLG on the dose rate was studied and the measurements were performed for five dose rates ranging from 200 to 600 MU/min, in steps of 100.

DLG_{EPID} Study

The EPID is supported by the EXaCT™ arm, centered on the machine isocenter, and has a sensitive area of 40 cm × 30 cm (1024 × 768 matrix) corresponding to a pixel size of 0.39 mm. The images were acquired in the "integrated image" mode at a SDD of 105 cm, with the image acquisition software 3 (IAS 3, version 7.5 Varian Medical Systems, Inc., USA) and Image Detection Unit-20 at a frame rate of 9.6 frames/s. The dark-field and flood-field corrections were performed to account for the background signals and the individual pixel insensitivity.[29]

The EPID images were acquired for all the DLG fields [Figure 3]. Since the EPID had already been calibrated for portal dosimetry, the EPID response was recorded as "calibrated unit" (CU). One CU corresponds

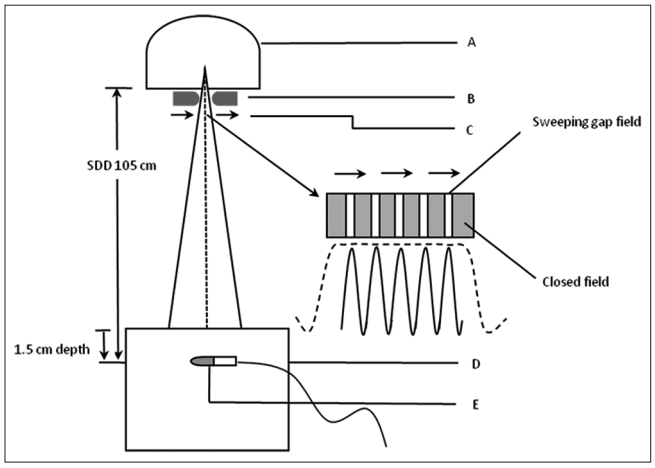

Figure 2: Schematic of DLG measurement using ionization chamber. (A) Gantry (B) MLC (C) Direction of sweeping beam. The magnified image shows the dose being delivered at different instances of the sweeping beam. A uniform dose (portrayed by the flat profile) is achieved as the result of the integrated dose. (D) Radiation field analyzer (E) Parallel orientation of ionization chamber (with respect to the direction of sweeping beam)

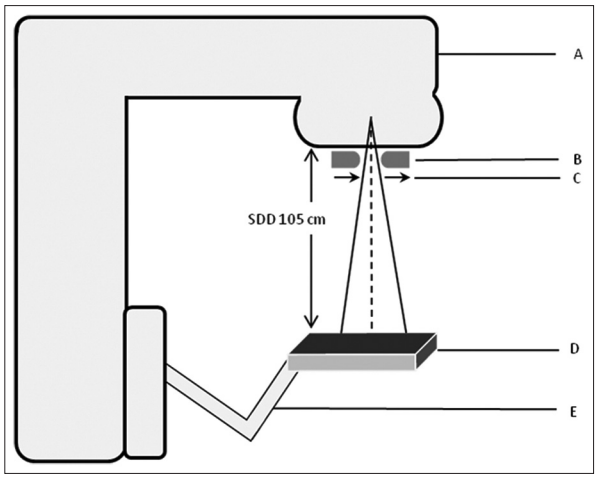

Figure 3: Schematic of DLG measurement using electronic portal imaging device (DLG_{EPID}). (A) Gantry (B) MLC with collimator at 90° (C) Direction of sweeping beam (D) aSi-EPID at SDD of 105 cm (E) EXaCT arm

to the integrated central pixel value when 1 cGy (1 MU) is delivered by the linear accelerator, with a reference field size of 10 cm × 10 cm at isocenter. Figure 4 shows the different regions of interest (ROIs) overlaid on the portal images of the sweeping gap fields. Initially, the CU values within the central ROI of 4 × 4 pixels of the EPID images were used to calculate the DLG_{EPID} as seen in Figure 4a.

However, ROIs were then selected on the basis of the volume and orientation of the ionization chamber. To relate back to results for the 0.125 cm^3 ionization chamber used in an orientation parallel to the direction of the sweeping beam, a 16 × 14 pixel ROI corresponding to the active area of the ionization chamber (6.5 mm × 5.5 mm) was used to measure the EPID doses. Similarly, for the perpendicular orientation, the ROI orientation was reversed (14 × 16 pixels), while a 14 × 14 pixel ROI was employed when the chamber was positioned parallel to CAX. Figure 4b and c show the EPID images acquired for the sweeping field with the ROI overlays (70 × 19 pixels and vice-versa) corresponding to the 0.6 cm^3 ionization chamber used in parallel and perpendicular orientations. Since the EPID response is dose rate dependent, the dose rate study was repeated with the EPID.

Dosimetric Impact of the Dosimetric Leaf Gap

The dosimetric influence of DLG on treatment planning was studied by recalculating three existing IMRT plans using LMC with the DLG values obtained using both the Farmer-type ionization chamber and EPID. Since the accuracy of the DLG value is reflected in the measurements performed on the treatment delivery machine, patient-specific QA viz., absolute dose measurements and fluence map verification using portal dosimetry were performed for the IMRT plans generated.

Results and Discussion

Since ionization chambers are the standard dosimeters used for the measurement of DLG, they were also used to validate the EPID measurements. The DLG values were derived from the extrapolation graph relating the corrected output $R_{(c, sg, w)}$ and the sweeping gap widths "w", as shown in Figure 5. The DLG_{ion} values determined with different volumes and orientations are listed in Table 1. The DLG_{ion} values derived from the graphs plotted were 1.133 mm and 1.107 mm for the 0.125 cm^3 and 0.6 cm^3 ionization chambers, when positioned perpendicular to the direction of the sweeping gap, and 1.120 mm and 1.083 mm for the direction parallel to the sliding window.

The MLC transmission values were relatively greater for the smaller volume chamber and resulted in higher DLG values as compared to the 0.6 cm^3 chamber for both orientations. The DLG_{ion} was found to be 1.157, while having an MLCT value of 1.394% for 0.125 cm^3 chamber (parallel to the CAX).

The dose profiles measured in parallel orientation across the interleaf region of a sweeping beam EPID image showed higher values than that of the intraleaf region [Figure 6]. In the case of the perpendicular orientation, sinusoidal lines of similar amplitudes were observed for both CAX and off-axis. The initial DLG_{EPID} was found to be 1.057 mm when the dose (in CU) was averaged over a central ROI of 4 × 4 pixels that falls in the interleaf region [Figure 4a]. Though this result was found to be closer to the DLG_{ion} value, it was not considered as it did not incorporate the intraleaf region that is included in the active volume of the ionization chamber measurement. Hence, the ROIs corresponding to the active areas of the ionization chambers in different orientations were used for determining the DLG_{EPID}.

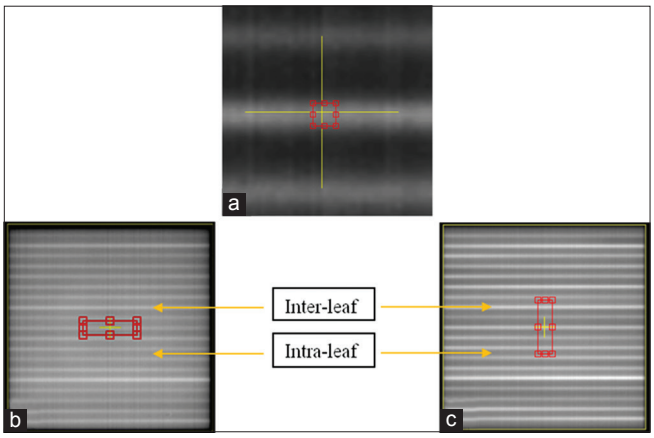

Figure 4: Different regions of interest (ROI) overlaid on the portal images of the sweeping gap fields (a) 4 × 4 pixels ROI in the interleaf region (b) and (c) ROI (70 × 19 pixels) for 0.6 cm³ ionization chamber with parallel and perpendicular orientations with respect to direction of sweeping beam

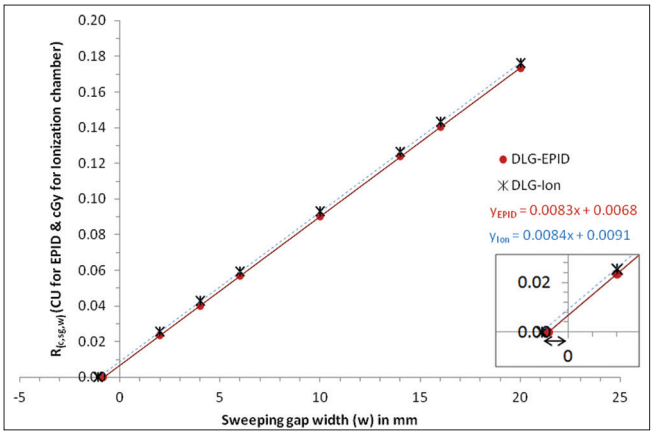

Figure 5: Extrapolation graph to calculate DLG_{EPID} and DLG_{ion} (0.125 cm³)

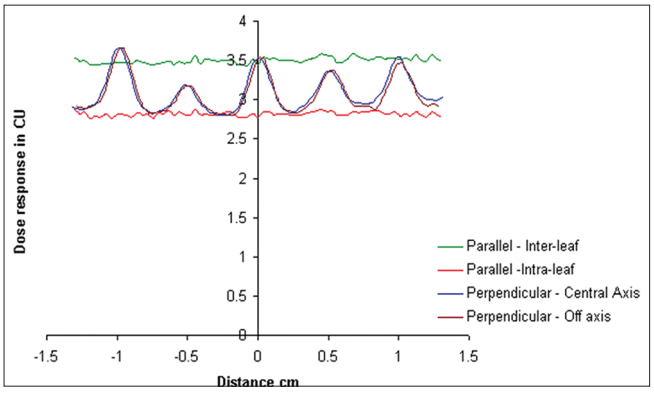

Figure 6: Dose profiles of sweeping gap field (2 mm width) acquired using the electronic portal imaging device

The DLG_{EPID} values, corresponding to the 0.125 cm³ chamber in different orientations viz., perpendicular (16 × 14 pixel ROI), parallel to the sweeping beam, and parallel to the CAX (14 × 14 pixels) were 0.843 mm, 0.819 mm, and 0.867 mm, respectively. For the 0.6 cm³ chamber, the DLG_{EPID} values were 0.807 mm and 0.735 mm for the orientations perpendicular and parallel to the sweeping beam. The overall standard deviation (SD) of 0.05 mm leads us to suggest that there was an averaging effect of the pixel values, which were spatially located over both the inter and intraleaf regions [Figure 4b and c]. However, it was noted that the DLG_{EPID}, corresponding to the 0.6 cm³ chamber was slightly higher for the perpendicular orientation as compared to that of the parallel orientation. This variation could be attributed to the former involving equal number of inter and intra-leaf regions, while the latter only had half the number of interleaf regions leading to lower DLG values. This was also observed in the DLG_{ion} values as mentioned above [Table 1].

Table 2 shows the DLG and MLCT values determined from "in water" and "in air" (with brass buildup) using the 0.6 cm³ chamber. While the results showed that the DLG_{ion} value was independent of the medium of measurement, the non-water-equivalent components of the EPID, such as the terbium-doped G_2O_2S phosphor, could also contribute to response of the EPID.[25]

All DLG_{EPID} images were acquired at SDD 105 cm at the detector depth of about 1.5 cm within the EPID. In order to simulate this, the DLG_{ion} was measured at d_{max} with SSD 103.5 cm and compared with the same at the standard SSD of 100 cm to study the influence of the small change in the detector distance. Though the small increment in the detector did not appreciably affect the DLG_{ion} value, they have been reported in Table 2. The EPID images were acquired with an inherent buildup of the water equivalent thickness of ~0.8 cm.[13] Additional buildup was not used.

Since the detection depth was 1.5 cm within the EPID, the same was simulated for the water phantom measurements. However, as the d_{max} is not the recommended depth for dose measurements, they were also carried out at 5 cm and 10 cm below the water surface. The DLG_{ion} and MLCT values for the three depths viz., 1.5 cm, 5 cm and 10 cm listed in Table 2 showed a marginal increase in DLG and MLCT values as a function of depth as also reported by Zygmanski *et al.*[12] However, the SD of 0.032 mm showed that the variation across the depths was negligible, thereby supporting the d_{max} measurement.

The DLG_{ion} and DLG_{EPID} values derived with different dose rates (200–600 MU/min) ranged from 1.048 to 1.121 mm (SD ± 0.03 mm) and 0.819 mm to 0.857 mm (SD ± 0.014 mm), respectively, as seen in Table 3. It could be noted that due to the constant MU settings, the velocity of the leaves changed as a function of dose rate, without affecting the dose delivery. The dependence of EPID signal on dose rate did not affect the DLG_{EPID} since the EPID calibration has been performed for each dose

Table 1: Impact of chamber volume and orientation on DLG

MLC parameter	Ionization chamber orientation					SD
	$\perp^r$ to sweeping beam		$\parallel^l$ to sweeping beam		$\parallel^l$ to CAX	
	0.125 cm^3	0.6 cm^3	0.125 cm^3	0.6 cm^3	0.125 cm^3	
DLG_{ion} (mm)	1.133	1.107	1.120	1.083	1.157	0.028
$MLCT_{ion}$ (%)	1.378	1.328	1.408	1.318	1.394	0.040
DLG_{EPID} (mm)	0.843	0.807	0.819	0.735	0.867	0.050
$MLCT_{EPID}$ (%)	1.045	1.096	1.061	1.042	1.045	0.023

SD: Standard deviation, DLG: Dosimetric leaf gap, MLC: Multileaf collimator, DLG_{ion}: Dosimetric leaf gap measured using ionization chamber, $MLCT_{ion}$: MLC transmission measured using ionization chamber, DLG_{EPID}: Dosimetric leaf gap measured using EPID, $MLCT_{EPID}$: MLC transmission measured using EPID, CAX: Central axis

Table 2: Dependence of DLG_{ion} on medium and depth of measurement and SSD

MLC parameter	Medium of measurement			SSD (cm)			Depth of measurement (cm)			
	Water	Air	SD	100	103.5	SD	1.5	5.0	10.0	SD
DLG_{ion} (mm)	1.107	1.131	0.017	1.096	1.108	0.032	1.096	1.108	1.157	0.032
$MLCT_{ion}$ (%)	1.328	1.375	0.033	1.302	1.328	0.031	1.302	1.328	1.363	0.031

DLG_{ion}: Dosimetric leaf gap measured using ionization chamber, $MLCT_{ion}$: MLC transmission measured using ionization chamber, SD: Standard deviation, SSD: Source to surface distance, MLC: Multileaf collimator

rate. However, this could be appreciable if the calibration of a nominal dose rate is applied to the measurements performed using other dose rates.

While the majority of DLG values found in the literature range from 1.9 to 2.4 mm,[4,5,9] lower values have also been recorded by Clark *et al.*[11] who reported DLG values of 1.05 mm and 0.97 mm. The DLG_{EPID} values in this study were lower when compared to the ionization chamber measurements. The combined plot of corrected output $R_{(c, sg, w)}$ Vs "w" for calculating the DLG_{ion} and DLG_{EPID} corresponding to the parallel orientation of the 0.125 cm^3 chamber is shown in Figure 5. It can be noted that, though the linear trends corresponding to both the EPID and ion data were very close to each other, the under-response of the EPID resulted in the straight line intercepting the x-axis at a lower value. The DLG_{EPID} was 0.26 mm lower than the DLG_{ion}, similar to the difference (0.3 mm) reported by Mei *et al.*,[13] due to the lower sensitivity of the EPID to smaller doses.

In order to study the influence of DLG on IMRT dose delivery, the measured DLG values were incorporated into the TPS. The DLG_{ion} of 1.083 mm (measured at nominal SSD with 0.6 cm^3 ionization chamber) resulted in the leaf tips being pulled back by 0.542 mm on either side of the MLC bank during the actual fluence calculation by the LMC that was performed for three existing IMRT plans. Subsequently, when the same was repeated for DLG_{EPID} of 0.819 mm, the leaf tips were further shifted by 0.132 mm inward on each side thereby reducing the calculated doses.

The patient-specific CAX dose measurements for the recalculated IMRT plans were performed using 0.6 cm^3 ionization chamber. For $DLG_{ion,}$ the difference between the measured and calculated doses were −0.05%, −4.71% and −5.22% for the three cases, while the same for DLG_{EPID} were found to be 1.67%, −2.04%, and 0.41%, respectively. The fluence map comparison results performed using portal dosimetry for both DLG_{ion} and DLG_{EPID} values-based IMRT plans are listed in Table 4. The QA results showed relatively close pixel pass rates for the fluence matrices with 3 mm distance to agreement and 3% dose difference gamma criteria.

Table 3: Dose rate dependence of DLG

DLG (mm)	Dose rate (MU/min)					
	200	300	400	500	600	SD
DLG_{EPID}	0.857	0.848	0.819	0.845	0.845	0.014
DLG_{ion}	1.120	1.048	1.108	1.121	1.095	0.030

DLG: Dosimetric leaf gap, DLG_{EPID}: Dosimetric leaf gap measured using EPID, DLG_{ion}: Dosimetric leaf gap measured using ionization chamber, SD: Standard deviation

Table 4: Gamma (γ) comparison of IMRT fields for plans with DLG_{EPID} and DLG_{ion}

Patient number	Number of fields	Mean pass % for $\gamma \leq 1$	
		DLG_{EPID}	DLG_{ion}
1	16	99.00	99.61
2	9	97.51	98.78
3	18	94.37	96.47

IMRT: Intensity modulated radiotherapy, DLG_{EPID}: Dosimetric leaf gap measured using EPID, DLG_{ion}: Dosimetric leaf gap measured using ionization chamber

Conclusion

While the dose maps of the sweeping fields obtained using EPID lend insight into the inter and intra-leaf patterns that fall into the active part of ionization chamber, it was found from both DLG_{EPID} and DLG_{ion} values that the DLG was independent of volume and orientation of the ionization chamber. It was also not influenced by the depth, SSD and the rate of dose delivery. Since the patient-specific QA tests showed comparable results between the DLG_{EPID} and

DLG_{ion}-based IMRT plans, it is concluded that the EPID as a high-resolution 2D detector which requires no elaborate setup, can be a suitable alternative in the determination of DLG. It also offers the prospect of determining and modeling the individual leaf DLG values for the entire leaf bank.

Acknowledgments

The authors would like to thank Mr. A. Sathish Kumar for his help with absolute dose measurements and Mr. L. Jose Solomon Raj for assisting with EPID image analysis.

Financial support and sponsorship

Nil.

Conflicts of interest

There is no conflicts of interest.

References

1. Aoki Y, Akanuma A, Karasawa K, Sakata K, Nakagawa K, Muta N, *et al*. An integrated radiotherapy treatment system and its clinical application. Radiat Med 1987;5:131-41.
2. Biggs PJ. Review of the improvements in the quality and applications of photon beams from linear accelerators in radiation therapy and a projection of future trends. Nucl Instrum Methods Phys Res Sect B Beam Interact Mater Atoms 1987;24-25:1096-9.
3. Ishigaki T, Sakuma S, Watanabe M. Computer-assisted rotation and multiple stationary irradiation technique. Newly designed overrunning multi-leaf collimators for conformation radiotherapy. Eur J Radiol 1988;8:76-81.
4. Arnfield MR, Siebers JV, Kim JO, Wu Q, Keall PJ, Mohan R. A method for determining multileaf collimator transmission and scatter for dynamic intensity modulated radiotherapy. Med Phys 2000;27:2231-41.
5. LoSasso T, Chui CS, Ling CC. Physical and dosimetric aspects of a multileaf collimation system used in the dynamic mode for implementing intensity modulated radiotherapy. Med Phys 1998;25:1919-27.
6. Saw CB, Siochi RA, Ayyangar KM, Zhen W, Enke CA. Leaf sequencing techniques for MLC-based IMRT. Med Dosim 2001;26:199-204.
7. Eclipse Algorithms Reference Guide. Palo Alto, CA: Varian Medical Systems, Inc.; 2011.
8. Srivastava SP, Das IJ, Kumar A, Johnstone PA. Dosimetric comparison of split field and fixed jaw techniques for large IMRT target volumes in the head and neck. Med Dosim 2011;36:6-9.
9. Van Esch A, Bohsung J, Sorvari P, Tenhunen M, Paiusco M, Iori M, *et al*. Acceptance tests and quality control (QC) procedures for the clinical implementation of intensity modulated radiotherapy (IMRT) using inverse planning and the sliding window technique: Experience from five radiotherapy departments. Radiother Oncol 2002;65:53-70.
10. Ezzell GA, Galvin JM, Low D, Palta JR, Rosen I, Sharpe MB, *et al*. Guidance document on delivery, treatment planning, and clinical implementation of IMRT: Report of the IMRT Subcommittee of the AAPM Radiation Therapy Committee. Med Phys 2003;30:2089-115.
11. Clark CH, Mubata CD, Meehan CA, Bidmead AM, Staffurth J, Humphreys ME, *et al*. IMRT clinical implementation: Prostate and pelvic node irradiation using Helios and a 120-leaf multileaf collimator. J Appl Clin Med Phys 2002;3:273-84.
12. Zygmanski P, Rosca F, Kadam D, Lrenz F, Nalichowski A, Chin L. Determination of depth and field size dependence of multileaf collimator transmission in intensity-modulated radiation therapy beams. J Appl Clin Med Phys 2007;8:2693.
13. Mei X, Nygren I, Villarreal-Barajas JE. On the use of the MLC dosimetric leaf gap as a quality control tool for accurate dynamic IMRT delivery. Med Phys 2011;38:2246-55.
14. Essers M, de Langen M, Dirkx ML, Heijmen BJ. Commissioning of a commercially available system for intensity-modulated radiotherapy dose delivery with dynamic multileaf collimation. Radiother Oncol 2001;60:215-24.
15. Thompson V, Bidmead M, Mubata C. Pictorial review: Comparison of portal imaging and megavoltage verification films for conformal pelvic irradiation. Br J Radiol 1996;69:1191-5.
16. Curtin-Savard A, Podgorsak EB. An electronic portal imaging device as a physics tool. Med Dosim 1997;22:101-5.
17. Budgell GJ, Zhang R, Mackay RI. Daily monitoring of linear accelerator beam parameters using an amorphous silicon EPID. Phys Med Biol 2007;52:1721-33.
18. Rowshanfarzad P, Sabet M, O'Connor DJ, Greer PB. Isocenter verification for linac-based stereotactic radiation therapy: Review of principles and techniques. J Appl Clin Med Phys 2011;12:3645.
19. Njeh CF, Caroprese B, Desai P. A simple quality assurance test tool for the visual verification of light and radiation field congruent using electronic portal images device and computed radiography. Radiat Oncol 2012;7:49.
20. Langmack KA. Portal imaging. Br J Radiol 2001;74:789-804.
21. van Herk M. Physical aspects of a liquid-filled ionization chamber with pulsed polarizing voltage. Med Phys 1991;18:692-702.
22. Kirby MC, Williams PC. Measurement possibilities using an electronic portal imaging device. Radiother Oncol 1993;29:237-43.
23. Louwe RJ, McDermott LN, Sonke JJ, Tielenburg R, Wendling M, van Herk MB, *et al*. The long-term stability of amorphous silicon flat panel imaging devices for dosimetry purposes. Med Phys 2004;31:2989-95.
24. McDermott LN, Louwe RJ, Sonke JJ, van Herk MB, Mijnheer BJ. Dose-response and ghosting effects of an amorphous silicon electronic portal imaging device. Med Phys 2004;31:285-95.
25. El-Mohri Y, Antonuk LE, Yorkston J, Jee KW, Maolinbay M, Lam KL, *et al*. Relative dosimetry using active matrix flat-panel imager (AMFPI) technology. Med Phys 1999;26:1530-41.
26. Street RA, Nelson S, Antonuk L, Perez Mendez V. Amorphous Silicon Sensor Arrays for Radiation Imaging. MRS Online Proc Libr 1990;192:441.
27. Antonuk LE, Boudry J, Huang W, McShan DL, Morton EJ, Yorkston J, *et al*. Demonstration of megavoltage and diagnostic x-ray imaging with hydrogenated amorphous silicon arrays. Med Phys 1992;19:1455-66.
28. Antonuk LE, Yorkston J, Huang W, Sandler H, Siewerdsen JH, el-Mohri Y. Megavoltage imaging with a large-area, flat-panel, amorphous silicon imager. Int J Radiat Oncol Biol Phys 1996;36:661-72.
29. Greer PB. Correction of pixel sensitivity variation and off-axis response for amorphous silicon EPID dosimetry. Med Phys 2005;32:3558-68.